NANO LETTERS

Letter

The Single Molecule Probe: Nanoscale Vectorial Mapping of Photonic Mode Density in a Metal Nanocavity

Jacob P. Hoogenboom, Gabriel Sanchez-Mosteiro, Gerard Colas des Francs, Dominique Heinis, Guillaume Legay, Alain Dereux, and Niek F. van Hulst

Nano Lett., **2009**, 9 (3), 1189-1195• DOI: 10.1021/nl803865a • Publication Date (Web): 16 February 2009

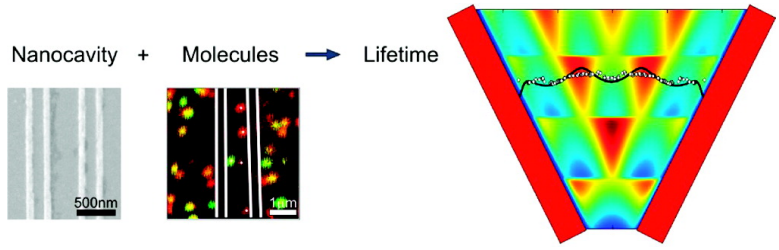

More About This Article

Additional resources and features associated with this article are available within the HTML version:

- Supporting Information
- Access to high resolution figures
- Links to articles and content related to this article
- Copyright permission to reproduce figures and/or text from this article

View the Full Text HTML

NANO LETTERS

2009
Vol. 9, No. 3
1189-1195

The Single Molecule Probe: Nanoscale Vectorial Mapping of Photonic Mode Density in a Metal Nanocavity

Jacob P. Hoogenboom,*,†,‡ Gabriel Sanchez-Mosteiro,† Gerard Colas des Francs,§ Dominique Heinis,† Guillaume Legay,§ Alain Dereux,§ and Niek F. van Hulst†,||

ICFO—Institut de Ciències Fotòniques, Av. Canal Olímpic s/n, E-08860 Castelldefels (Barcelona), Spain, Soft Condensed Matter, Debye Institute for Nanomaterials Research, Utrecht University, Utrecht, The Netherlands, Institut Carnot de Bourgogne, CNRS UMR 5209—Université de Bourgogne, 9 avenue A. Savary, F-21078 Dijon, France, ICREA—Institució Catalana de Recerca i Estudis Avançats, E-08015 Barcelona, Spain

Received December 22, 2008; Revised Manuscript Received February 4, 2009

ABSTRACT

We use superresolution single-molecule polarization and lifetime imaging to probe the local density of states (LDOS) in a metal nanocavity. Determination of the orientation of the molecular transition dipole allows us to retrieve the different LDOS behavior for parallel and perpendicular orientations with respect to the metal interfaces. For the perpendicular orientation, a strong lifetime reduction is observed for distances up to 150 nm from the cavity edge due to coupling to surface plasmon polariton modes in the metal. Contrarily, for the parallel orientation we observe lifetime variations resulting from coupling to characteristic $\lambda/2$ cavity modes. Our results are in good agreement with calculations of the nanoscale variations of the projected LDOS, which demonstrates the potential of single molecules as nonperturbative, nanoscale vectorial point probes in photonic and biological nanostructures.

Recent advances in high-resolution optical microscopy have highlighted the possibility of truly nanoscopic, subdiffraction limited, far-field imaging using single fluorescent probes.[1] Novel modalities like photoactivated localization microscopy (PALM)[2] and stochastic optical reconstruction microscopy (STORM)[3,4] rely on confinement of the fluorescence emission down to the level of a single molecule. By collection of a statistically sound number of photons from each single emitter sequentially, their individual positions can be retrieved resulting in a spatial resolution on the order of 20 nm.[5,6] While the possibility to image spatial structure with nanoscopic resolution already presents an important breakthrough, the intrinsic multiparameter character of fluorescence emission provides a means to also acquire functional information with nanometer-scale precision. For instance, using different labeling strategies for spectrally shifted fluorophores, biological functionality can be mapped onto spatial structure.[7,8] So far, however, the *intrinsic* variations in single-molecule fluorescence properties due to variations in the local nanoenvironment of the emitters have been only sparsely exploited in combination with high-resolution spatial imaging.[9] As we will demonstrate in this Letter, this scheme provides a means to acquire detailed spatial, and in addition vectorial, functional information, in our case on the mode density in photonic nanostructures.

The fluorescence characteristics of a molecule are determined by both the internal energy level diagram and the external photonic local density of states (LDOS), as expressed by the well-known Fermi golden rule.[10] Since the pioneering work of Drexhage[11] the distance-dependent lifetime variations near mirror and grating planes have been investigated by positioning a bulk amount of europium fluorophores at fixed distances using nanometric polymer Langmuir—Blodgett multilayers.[12,13] In recent years, the ability to create photonic structures with nanometric position control has led to a renewed interest in fluorescence lifetime and spectra control through tailored modification of the LDOS. Controlled emission in systems like nanoantennas, cavities, photonic bandgap materials, and plasmon nanostructures holds promise for applications in sensing, light harvesting and energy conversion, photon sources, and quantum computation. Indeed, modification of lifetime,[14−23] spectra,[17,24,25] emission directivity,[26] and intersystem crossing

* Corresponding author, j.p.hoogenboom@tudelft.nl. Present address: Department of Imaging Science and Technology, Faculty of Applied Physics, Delft University of Technology, Delft, The Netherlands.
† ICFO.
‡ Debye Institute.
§ Institut Carnot de Bourgogne.
|| ICREA.

10.1021/nl803865a CCC: $40.75
Published on Web 02/16/2009

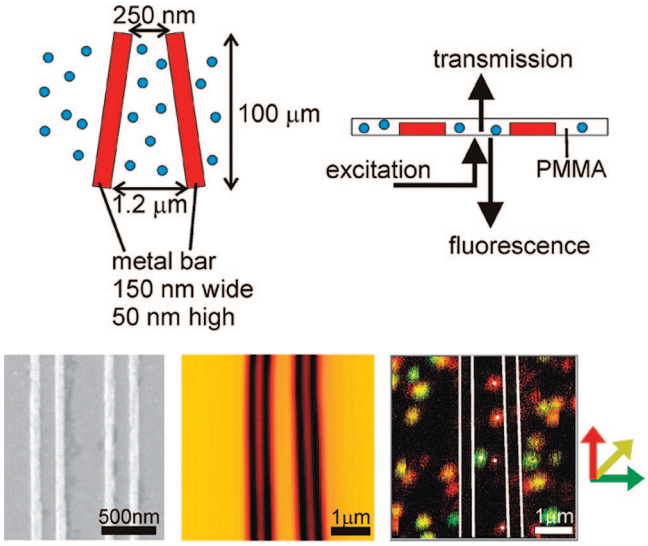

Figure 1. Schematic indication of the cavity design and relevant experimental parameters. Upper left part of the figure shows a top view of the cavity structure where red stripes indicate the gold bars and blue dots the randomly positioned molecules. Upper right part shows a side view with the relevant excitation and detection light paths indicated. Bottom left shows a SEM image of the metal mirror cavity prior to deposition of the polymer and molecules. Three cavity structures were fabricated next to each other: spacing between first and second and third and fourth metal bar was kept constant at 250 nm, the spacing between the second and third bar was gradually increased as indicated in the upper left image. The 150 nm width of the gold bars prevents long-range interactions between molecules located in adjacent cavities. The cavity structure is imaged in transmission mode (middle image) while DiD molecules are simultaneously imaged in fluorescence mode (bottom right). Retrieved positions of mirror planes and molecules are indicated with white stripes and dots. Red and green color coding in the fluorescence image refers to orthogonal emission polarization directions as indicated by the arrows.

rates[27] has recently been explored. However, while experiments on single fluorophores positioned in a cavity have recently been reported,[17,23,24,28,29] the high-resolution single-molecule spatial accuracy has not yet been used in combination with retrieval of such functional information. While several alternative techniques to probe the LDOS in photonic nanostructures have been proposed,[30,31] direct measurement using fluorophores[32] ultimately yields nanoscopic spatial resolution. Embedding the nanoscopic molecular probe in the cavity structure, bears the further advantage that the probe itself does not in turn perturbate the LDOS.[33] In addition, the fixed transition dipole moment of an immobilized molecule holds the clear advantage of probing the LDOS in a vectorial fashion.

Here, we use high-resolution single-molecule fluorescence lifetime imaging to spatially and vectorially probe the LDOS in a metallic nanocavity. This provides us with a full vectorial lifetime-LDOS map throughout the nanocavity. Our results are compared to the expected behavior based on direct calculations of the projected LDOS inside the cavity.

The two-dimensional nanocavity we investigated consists of two gold bars, each of 150 nm width and 50 nm height, fabricated by electron-beam lithography on an indium tin oxide substrate using a standard lift-off procedure. On the samples, three nanocavities were fabricated next to each other, the outer with a fixed width of 250 nm, the middle one with width varying between 250 nm and 1.2 μm. The layout is schematically indicated in Figure 1. By spin coating from a toluene solution, the structure was embedded in a 60 nm high poly(methyl methacrylate) (PMMA) film containing about 10^{-8} M of fluorescent 1,1′-dioctadecyl-3,3,3′,3′-tetramethylindocarbocyanine perchlorate (DiD, Invitrogen) molecules. The thickness of the PMMA film was chosen to be larger than the height of the mirror bars in order to minimize curvature of the polymer−air interface in the cavity, while still maintaining a sufficiently thin film to avoid focal overlap of molecules located at different heights in the film. The quantum yield of DiD is 1, which means that unless additional nonradiative decay channels are opened such as quenching in very close proximity (<10 nm) to the metal surface, lifetime changes are reminiscent of changes in the radiative decay rate. The structure was imaged in optical transmission and fluorescence simultaneously (as indicated in Figure 1) using a home-built confocal microscope. Excitation was performed using a 635 nm diode laser (Picoquant LDH-635, 90 ps fwhm, 20 MHz). Fluorescence light was separated from reflected excitation light using a dichroic mirror (Omega 650DRLP) and a 665 nm long pass filter (Omega 665ALP), split by a polarization cube and collected on two avalanche photodiodes (APD, EG&G Electro Optics SPCM-AQ-14) connected to a time-correlated single photon counting card (TCSPC, Picoquant Timeharp 200). Images were acquired using a reduced power density of 0.11 kW/cm^2 to avoid rapid photobleaching, with a pixel size of 39 × 39 nm^2 and a 1 ms dwell time. After image scanning, fluorescence from selected single-molecule locations was collected by continuous excitation at 3 kW/cm^2. Single-molecule positions were extracted from the fluorescence image by applying a Gaussian filter followed by calculation of the center-of-mass for selected molecular intensity profiles (see Figure 1). The fluorescence lifetime was calculated from the intensity time trace recorded for a specific molecule by constructing the histogram of photon arrival times and fitting to a single-exponential decay. Both positional[5] and lifetime accuracy[34] are dependent on the number of detected photons. For the highly photostable DiD molecule (typically 10^4−10^5 detected photon counts), we have molecular positional accuracy ∼30 nm, and lifetime accuracy ∼0.1 ns. Positions of the metal mirror bars were retrieved from the transmission image. In addition to the high-resolution determination of dipole position and lifetime, the polarization-sensitive detection of emission light allows us to also determine the orientation of the dipole emitter.

Measured position- and orientation-dependent fluorescence lifetimes are compared to the outcome of LDOS calculations. For an emitter with a fixed transition dipole moment, like our immobilized DiD molecules, the fluorescence decay rate Γ—the inverse of the lifetime—is related to the projected LDOS (pLDOS) through Fermi's golden rule[10]

$$\Gamma(\mathbf{r}) = \frac{\pi\omega}{\hbar\varepsilon_0}|\mu|^2\rho_u(\mathbf{r},\omega)$$

where r is the position of the emitter, ω its resonance frequency, μ the transition dipole moment, and ρ_u the pLDOS along the direction $\mathbf{u}$ of the transition dipole moment $\boldsymbol{\mu} = \mu\mathbf{u}$. The pLDOS is determined using Green's dyad formulation.[35] In order to take into account the unknown transition dipole moment in Fermi's golden rule, the decay rate relative to a reference decay rate is calculated. As a reference we take the average decay rate for DiD molecules in a thin PMMA film. We will see below that this reference also allows us to take into account the intrinsic heterogeneity in the experimental single-molecule lifetime distribution.

In total, we extracted positions and lifetimes inside the cavity for 880 DiD molecules. The position in the cavity was defined as the distance to the nearest cavity edge. In Figure 2a the single-molecule lifetime as a function of position inside cavity is given. As can be seen, the distribution of lifetimes broadens and shifts to lower values with decreasing distance to a mirror. In addition to the cavity molecules, we measured 158 DiD molecules at a macroscopic distance from the mirror cavities to extract the reference. This reference distribution, yielding an averaged DiD lifetime of 2.6 ns, is indicated in Figure 2b together with the full distribution for the cavity molecules. Here, we note a clear shift of the distribution average to lower lifetime values as well as a broadening toward even lower, sub-1-ns lifetimes

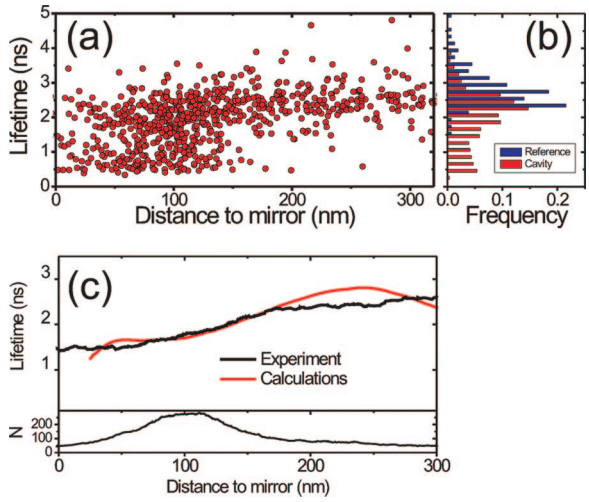

Figure 2. (a) Lifetime as a function of distance to the nearest mirror bar for all 880 molecules measured inside the mirror cavity. (b) Distribution of fluorescence lifetimes for all these cavity molecules (in red), compared to the reference histogram of 158 molecules measured far away from the cavity structure. The reference histogram shows the effects of intrinsic molecular variations in the lifetime due to, e.g., variations in the local nanoenvironment of the molecules, and the finite size of the PMMA film and the proximity of the glass plate. Compared to the reference distribution, the distribution of lifetimes in the cavity is markedly shifted to lower values, with a tail extending to sub-1-ns values. (c) Average lifetime as a function of distance to the nearest mirror (black line) compared to the expected lifetime behavior based on LDOS calculations (red line). Both experimental and calculated curves have been retrieved by applying a 50 nm averaging window and are averaged over all orientations and cavity sizes. The lower panel indicates the number of experimental data points (i.e., molecules) in the averaging window as a function of distance.

for the cavity molecules. This result along with Figure 2a strongly indicates position-dependent lifetime modifications for molecules located inside the cavity.

A second point to note here is that the reference distribution of "free" molecules already shows broadening and thus lifetime variations from molecule to molecule. This broadening is predominantly caused by the proximity of polymer−air and polymer−glass interfaces due to the finite size of the PMMA film. These interfaces lead to modifications in the LDOS and thus in fluorescence lifetimes for molecules at different heights in the film and with different out-of-plane orientations[36] (note that in the polarization-sensitive fluorescence image in Figure 1, we measure the molecular orientation projected onto the substrate). In addition, small variations in lifetime from molecule to molecule may be caused by variations in the local nanoenvironment.[37] Thus, in order to extract position-dependent information on molecular lifetime variations, one has to either measure the same molecule in different conditions, which is rather cumbersome but could in principle be performed with a scanning probe microscope[18,19,26] or an ion trap,[28] or one has to explicitly take into account the distributed lifetimes, as we will do in the following.

First, we construct a position-dependent average lifetime, by averaging the data in Figure 2a with a 50 nm window. The result is indicated in Figure 2c, together with the expected lifetime behavior based on LDOS calculations. In the calculations, we consider a 1D cavity, neglecting the finite height of the cavity. Note that refractive indices of substrate and polymer film are very similar (around 1.5) and that molecular lifetime variation due to the finite polymer thickness will be accounted for in the experimental results by comparison to the reference distribution. In Figure 2c, we observe a good agreement between the experimental and calculated results, indicating that the observed modifications in molecular lifetime distributions are indeed due to the modified LDOS inside the cavity. At this point, however, we have to bear in mind that data are averaged over all molecular orientations and all cavity widths. These two points will be disentangled consecutively.

Now, we note that a different lifetime behavior may be expected for molecules with a transition dipole moment located parallel and perpendicular to the mirrors (indicated in Figure 3a). The molecular dipole orientation can be evaluated from the measured fluorescence polarization by defining the degree of polarization $P = (I_r - I_g)/(I_r + I_g)$, where I_r and I_g denote detected intensity on red and green APD channels, respectively (see also lower right image in Figure 1). Figure 3a depicts the histogram of degree of polarization for all cavity molecules. Now, we define the subsets of parallel and perpendicular oriented molecules as indicated in Figure 3a. For both these subsets we apply the same procedure with a 50 nm integration window as above to plot the molecular lifetime as a function of distance to the mirror (Figure 3b). A clearly different behavior for parallel compared to perpendicular molecules can be observed. Most notably, the strong decrease in lifetime for distances <100 nm to the mirror is mostly due to perpen-

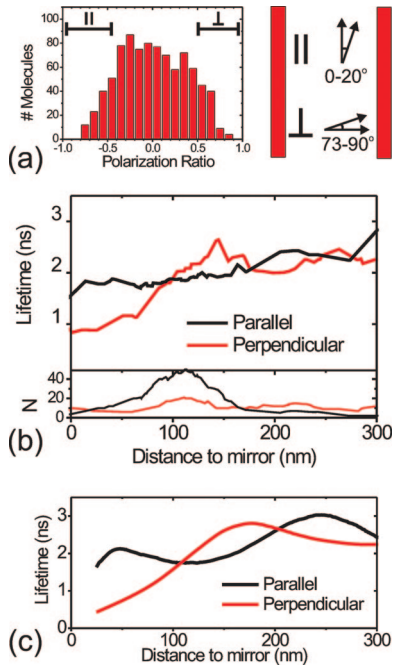

Figure 3. (a) Histogram of the degree of polarization of all 880 molecules inside the cavity structure. For vectorial probing the cavity LDOS, we look at two subdistributions, which are defined by their relative orientation with respect to the cavity design, as indicated in the drawing. For selecting both parallel and perpendicular sets of molecules, the outmost 12.5% of molecules on both sides of the distribution were taken (102 parallel, 85 perpendicular). (b) Measured fluorescence lifetime as a function of distance to the nearest mirror for both distributions of molecules oriented parallel and perpendicular to the mirror. The lower panel indicates the number of molecules within the 50 nm averaging window as a function of distance. (c) Calculated dependence of the lifetime on distance to the mirror for both orientations. There is a good agreement between experimental and calculated results in terms of the strong reduction of lifetime for perpendicular orientation for distances below 100 nm, the more gradual increase of lifetime away from the mirror for the parallel orientation, and the crossover between parallel and perpendicular curves at ~100 nm and ~190 nm.

dicular oriented molecules, while the parallel molecules display a more gradual decrease with decreasing distance to one of the mirrors. In addition, comparing both curves to the results based on LDOS calculations (given in Figure 3c), we see that the relative behavior of both curves is in correspondence with the theoretical predictions. Thus, the fixed transition dipole moment of an immobilized molecule is found to reproduce LDOS variations in a *vectorial* fashion; i.e., it probes the *projected* LDOS (pLDOS).

Next, we turn to the behavior for both orientations for different cavity sizes. We note that different behavior may be expected for cavities that differ in size by integer times half the effective wavelength, $i \cdot \lambda/2n = i \cdot 223$ nm, with $\lambda = 665$ nm and $n = 1.49$. In Figure 4 the calculated pLDOS and corresponding lifetimes for all cavity sizes and all positions within the cavity are shown. A clear difference for dipoles oriented parallel with respect to the axis compared to those with a perpendicular orientation can be observed over the full range of cavity widths. This difference originates from coupling to two different types of modes in the nanocavity. For a parallel orientation, the pLDOS, depicted in Figure 4a, is dominated by Fabry−Perot type cavity modes (see Supporting Information). Here, the number of maxima increases with i as expected. Thus, for $i = 1$, i.e., cavity size $\lambda/2n < d < \lambda/n$, we observe a single maximum in the pLDOS at the cavity center. For very small distances (<10 nm) to the metal edge, strong nonradiative decay due to quenching to the metal takes place leading to a steep increase of the pLDOS. At positions equal to 0.25 and 0.75 of the size of the $i = 1$ cavity, pLDOS is at a minimum. For $i = 2$, $\lambda/n < d < 3\lambda/2n$, two maxima in the pLDOS are observed, and so on for increasing i. Note that the actual values are slightly smaller than $i \cdot \lambda/2n$ due to the penetration depth in the metal.[38] The pLDOS translates into inverse behavior for the fluorescence lifetime as indicated in Figure 4b for a parallel oriented dipole.

For the perpendicular orientation, given in panels c and d of Figure 4, an entirely different behavior is observed. In this case the pLDOS is dominated by surface plasmon polariton (SPP) modes in the metal edges[35,39] (see Supporting Information), which, for distances <150 nm from the edge, leads to a gradual decrease in lifetime when approaching one of the edges. At distances >150 nm, the fluorescence lifetime is basically unaffected by the presence of the metallic nanocavity.

We compare the pLDOS calculations with our experimental data for two different cavity types, namely, the smallest one ($i = 1$) and the $i = 3$ cavity. These are indicated with dashed lines in Figure 4. In the experimental data we collect all molecules in cavity size range supporting these mode types, i.e., $0.45\lambda/n < d < 0.67\lambda/n$ for the $i = 1$ cavity and $1.40\lambda/n < d < 1.90\lambda/n$ for the $i = 3$ cavity. These values deviate slightly from integer times $\lambda/2n$ due to the penetration depth in the metal and the fact that we exclude the region close to the mode cutoff. For the $i = 3$ cavity, the criteria for parallel and perpendicular molecules was increased to respectively $P < -0.05$ and $P > 0.05$ to have sufficient molecules in each subset (66 and 93, respectively, compared to 115 and 48, respectively, for the (shorter) $i = 1$ cavity), where we verified that applying these criteria to the entire set of molecules, the curves in Figure 3 remained unchanged.

The experimental data for the lifetime as a function of distance to the nearest mirror is given in Figure 5, together with the theoretical results for cavity sizes of $d = 225$ and 670 nm, respectively, which correspond to the positions indicated by dashed lines in Figure 4. For the $i = 1$ cavity, it can be seen that the lifetime at every position in the cavity for both orientations is reduced compared to the average lifetime in the reference distribution (indicated by the dashed line) in correspondence with the lifetime calculations and the strong increase in pLDOS in Figure 4c. Moreover, we see that while for the parallel orientation the lifetime only shows small variations between $\tau = 1.5$ ns and $\tau = 2$ ns, the perpendicular orientation displays even lower lifetime values which gradually decrease below 1 ns upon approaching the mirror. As the response time of the APD is of the order of 200−400 ps, the few molecules in the 50 nm averaging window with relatively longer lifetimes dominate

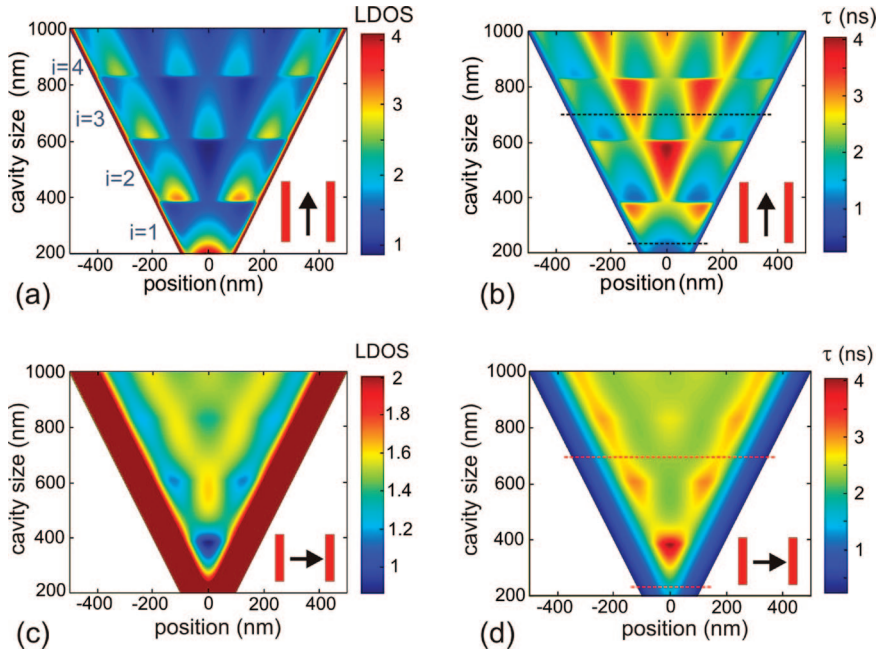

Figure 4. (a) Calculated pLDOS in the direction parallel to the cavity interfaces, as a function of both position in the cavity and cavity size. (b) Corresponding fluorescence lifetime for a DiD fluorescent molecule oriented parallel with respect to the cavity. (c) pLDOS and (d) DiD lifetime for a perpendicular orientation. The pLDOS is normalized with respect to the free space value, its color scale is saturated with maxima reaching 15 for parallel (top left) and 35 for perpendicular orientation (bottom left). Indicated in the top left image are the cavity types i that group cavity sizes based on the number of sustained modes. A clear difference between both dipole orientations can be seen, which results from predominant coupling to cavity modes for a parallel orientation compared to coupling to SPP modes for the perpendicular orientation. Dashed lines indicate the location of the curves shown in Figure 5.

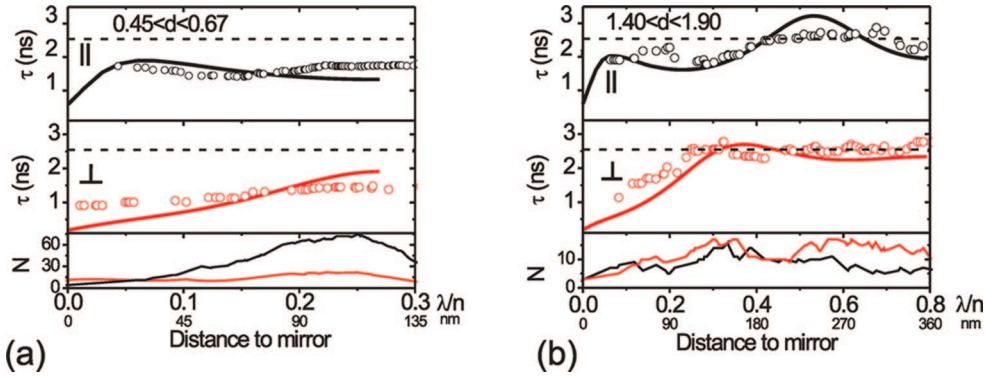

Figure 5. Average lifetime as a function of position to the nearest metal mirror plane for the two cavity sizes indicated in Figure 4. Cavity size is indicated in reduced units (relative to the effective wavelength in the PMMA matrix), which corresponds to (a) cavity type $i = 1$ (interval of $200 < d < 300$ nm), and (b) cavity type $i = 3$ ($625 < d < 850$ nm). Open dots refer to the molecular lifetime, averaged over the indicated range of cavity sizes and a 50 nm window in position; the solid lines refer to the calculated lifetime for a cavity size halfway the experimental interval. Top panels (black curves and dots) are for a dipole orientated parallel to the mirror, middle panels (red curves and dots) for a perpendicular dipole orientation. The lower panels indicate the number of molecules in the averaging. The dashed lines indicate the average fluorescence lifetime without cavity structure. For both cavity sizes a clear difference between the two dipole orientations can be observed, closely following the expected behavior based on the LDOS calculations.

the averaging. Thus our averaged experimental lifetime data has a lower limit of ~1 ns, while the calculated result decays toward zero.

For the $i = 3$ cavity, we observe a different behavior with smaller reduction of fluorescence lifetime due to smaller LDOS variations in line with the results from the calculations. At comparatively larger distance from the mirror, the lifetime is about equal to its reference value with, for the parallel case, a reduction to 2 ns for distances smaller than about 200 nm ($0.45\lambda/n$) as well as very close to the cavity center. For the perpendicular orientation, fluorescence lifetime is only modified from the reference value for distances smaller than 110 nm ($0.25\lambda/n$), where it steadily decreases to zero due to coupling to the SPP mode in the metal like for the $i = 1$ cavity. All in all, we observe clearly different behavior for both cavity sizes and for both orientations, in all cases in line with the expected lifetime behavior based on pLDOS calculations. Thus we conclude that our single-molecule lifetime

measurements map the LDOS with vectorial sensitivity at nanometer-scale, single-molecule spatial resolution.

The approach presented here, relying on superresolution, single-molecule, spatial imaging of fluorescence lifetime and polarization anisotropy, can be highly relevant for biological systems, extending the possibilities of novel nanoscopy techniques[1] like PALM[2] and STORM.[3,4] While polarization-sensitive superresolution microscopy, based on fluorescence photoactivation (P-FPALM),[40] has very recently been demonstrated, the inclusion of fluorescence lifetime measurements[41] truly exploits the multiparameter character of molecular fluorescence for unraveling biological structure and functionality at the nanoscale. The vectorial information gives access to (locally restricted) rotational diffusion, and thus viscosity, and to emerging orientational and positional ordering. Note that this holds both for situations where the molecular transition dipole moment is fixed, like in our study, and those situations where it is not. The latter case also allows a single molecule to probe part of the orientation and position phase space; however, it should be noted that this comes at the expense of position accuracy, which directly depends on the number of detected photon counts. Adding to the vectorial information, molecular fluorescence lifetime variations may be related to differences in the biochemical environment of the probe or to binding or energy transfer events. Moreover, fluorescence lifetime is an important discriminator between different fluorophores and can thus be used to map functionality using different labeling strategies. Clearly, correlating lifetime and orientation data, like in our nanophotonics structure, extends these capabilities, for instance revealing orientation-dependent interactions and transfer processes in biomolecular machinery.

In our study, we have an estimated average accuracy of $\sim$30 nm in position and $\sim$0.1 ns in lifetime. For localization microscopy using photoactivated fluorophores, position resolution of $\sim$20 nm has been reported. Both position and lifetime resolution are dependent on the number of detected photon counts[5,34] and thus mostly limited by photobleaching. The use of photobleaching-resistant quantum dots, or anisotropic quantum rods, would allow for detection of a fixed, aimed number of photon counts, and could push this resolution to 10 nm, if photoblinking[42] can be substantially prevented. With respect to lifetime, we currently encounter a lower limit of $\sim$0.5 ns, set by a detector response time of 200−400 ps, compared to an average molecular fluorescence lifetime of 2.6 ns. Here, the tens of nanoseconds or larger lifetime of quantum dots would considerably increase the dynamic range, which would for instance be important in probing strong quenching close to the metal interface. However, care should be taken to properly analyze and interpret the multiexponential decay of single quantum dots.[43,44]

In summary, we have presented the use of single fluorescent molecules as local nanoscopic probes for the LDOS in a metallic nanocavity, mapping the full position- and cavity-size-dependent lifetime LDOS curve. The single-molecule probe holds the demonstrated advantages of vectorial sensitivity and ultimate nanometer-scale spatial resolution; i.e., it is a vectorial point-probe. In addition, probing is performed in a nonperturbative fashion. Thus, this approach has the promising perspective of probing functional nanophotonic structures like nanoantennas, photonic crystals, high-Q resonators, and sensors based on near-field enhancement. In addition, the methodology can be relatively straightforwardly extended to the probing of nanofocusing effects, local field enhancement, and enhanced quantum efficiency in such structures. Finally, as discussed, the concept of superresolution single-molecule fluorescence lifetime, and polarization imaging has great prospects for nanoscopy of biological systems.

Acknowledgment. The authors thank Aude Lereu for assistance with the sample preparation. This work was supported in part by the European Network of Excellence (NoE) Plasmonanodevices, the Stichting voor Fundamenteel Onderzoek der Materie (FOM), and the STREP ASPRINT in the EU 6th framework.

Supporting Information Available: Results of a plane wave expansion of the emitted power of a dipole in relation to its position and orientation in the nanocavity, which reveals the magnitude of coupling to cavity and SPP modes. This material is available free of charge via the Internet at http://pubs.acs.org.

References

(1) Hell, S. W. *Science* **2007**, *316* (5828), 1153–1158.
(2) Betzig, E.; Patterson, G. H.; Sougrat, R.; Lindwasser, O. W.; Olenych, S.; Bonifacino, J. S.; Davidson, M. W.; Lippincott-Schwartz, J.; Hess, H. F. *Science* **2006**, *313* (5793), 1642–1645.
(3) Huang, B.; Wang, W. Q.; Bates, M.; Zhuang, X. W. *Science* **2008**, *319* (5864), 810–813.
(4) Bates, M.; Huang, B.; Dempsey, G. T.; Zhuang, X. W. *Science* **2007**, *317* (5845), 1749–1753.
(5) Thompson, R. E.; Larson, D. R.; Webb, W. W. *Biophys. J.* **2002**, *82* (5), 2775–2783.
(6) Qu, X. H.; Wu, D.; Mets, L.; Scherer, N. F. *Proc. Natl. Acad. Sci. U.S.A.* **2004**, *101* (31), 11298–11303.
(7) Churchman, L. S.; Okten, Z.; Rock, R. S.; Dawson, J. F.; Spudich, J. A. *Proc. Natl. Acad. Sci. U.S.A.* **2005**, *102* (5), 1419–1423.
(8) Bossi, M.; Fölling, J.; Belov, V. N.; Boyarskiy, V. P.; Medda, R.; Egner, A.; Eggeling, C.; Schönle, A.; Hell, S. W. *Nano Lett.* **2008**, *8* (8), 2463–2468.
(9) van Oijen, A. M.; Kohler, J.; Schmidt, J.; Muller, M.; Brakenhoff, G. J. *J. Opt. Soc. Am. A* **1999**, *16* (4), 909–915.
(10) Fermi, E. *Rev. Mod. Phys.* **1932**, *4*, 87.
(11) Drexhage, K. *J. Lumin.* **1970**, *1,2*, 693–701.
(12) Amos, R. M.; Barnes, W. L. *Phys. Rev. B* **1997**, *55* (11), 7249–7254.
(13) Andrew, P.; Barnes, W. L. *Phys. Rev. B* **2001**, *64* (12), 125405.
(14) Kleppner, D. *Phys. Rev. Lett.* **1981**, *47* (4), 233–236.
(15) Goy, P.; Raimond, J. M.; Gross, M.; Haroche, S. *Phys. Rev. Lett.* **1983**, *50* (24), 1903–1906.
(16) Lodahl, P.; van Driel, A. F.; Nikolaev, I. S.; Irman, A.; Overgaag, K.; Vanmaekelbergh, D.; Vos, W. L. *Nature* **2004**, *430* (7000), 654–657.
(17) Steiner, M.; Schleifenbaum, F.; Stupperich, C.; Failla, A. V.; Hartschuh, A.; Meixner, A. J. *ChemPhysChem* **2005**, *6*, 2190–2196.
(18) Kuhn, S.; Hakanson, U.; Rogobete, L.; Sandoghdar, V. *Phys. Rev. Lett.* **2006**, *97*, 017402.
(19) Anger, P.; Bharadwaj, P.; Novotny, L. *Phys. Rev. Lett.* **2006**, *96* (11), 113002.
(20) Tam, F.; Goodrich, G. P.; Johnson, B. R.; Halas, N. J. *Nano Lett.* **2007**, *7* (2), 496–501.
(21) Muskens, O. L.; Giannini, V.; Sánchez-Gil, J. A.; Gómez-Rivas, J. *Nano Lett.* **2007**, *7* (9), 2871–2875.
(22) Buchler, B. C.; Kalkbrenner, T.; Hettich, C.; Sandoghdar, V. *Phys. Rev. Lett.* **2005**, *95* (6), 4.
(23) Lund-Hansen, T.; Stobbe, S.; Julsgaard, B.; Thyrrestrup, H.; Sunner, T.; Kamp, M.; Forchel, A.; Lodahl, P. *Phys. Rev. Lett.* **2008**, *101*, 113903.

(24) Barth, M.; Schuster, M.; Gruber, A.; Cichos, F. *Phys. Rev. Lett.* **2006**, *96*, 243902.
(25) Ringler, M.; Schwemer, A.; Wunderlich, M.; Nichtl, A.; Kurzinger, K.; Klar, T. A.; Feldmann, J. *Phys. Rev. Lett.* **2008**, *100*, 203002.
(26) Taminiau, T. H.; Stefani, F. D.; Segerink, F. B.; Van Hulst, N. F. *Nat. Photonics* **2008**, *2* (4), 234–237.
(27) Stefani, F. D.; Vasilev, K.; Bocchio, N.; Gaul, F.; Pomozzi, A.; Kreiter, M. *New J. Phys.* **2007**, *9*, 21.
(28) Guthohrlein, G. R.; Keller, M.; Hayasaka, K.; Lange, W.; Walther, H. *Nature* **2001**, *414* (6859), 49–51.
(29) Steiner, M.; Failla, A. V.; Hartschuh, A.; Schleifenbaum, F.; Stupperich, C.; Meixner, A. J. *New J. Phys.* **2008**, *10*, 123017.
(30) Chicanne, C.; David, T.; Quidant, R.; Weeber, J.-C.; Lacroute, Y.; Bourillot, E.; Dereux, A.; Colas des Francs, G.; Girard, C. *Phys. Rev. Lett.* **2002**, *88*, 097402.
(31) Huang, C.; Bouhelier, A.; Colas des Francs, G.; Legay, G.; Weeber, J.-C.; Dereux, A. *Opt. Lett.* **2008**, *33* (4), 300–302.
(32) Koenderink, A. F.; Kafesaki, M.; Soukoulis, C. M.; Sandoghdar, V. *Opt. Lett.* **2005**, *30* (23), 3210–3212.
(33) Mujumdar, S.; Koenderink, A. F.; Sunner, T.; Buchler, B. C.; Kamp, M.; Forchel, A.; Sandoghdar, V. *Opt. Express* **2007**, *15* (25), 17214–17220.
(34) Köllner, M.; Wolfrum, J. *Chem. Phys. Lett.* **1992**, *200* (1−2), 199–204.
(35) Barnes, W. L. *J. Mod. Opt.* **1998**, *45* (4), 661–699.
(36) Vallee, R.; Tomczak, N.; Gersen, H.; van Dijk, E.; Garcia-Parajo, M. F.; Vancso, G. J.; van Hulst, N. F. *Chem. Phys. Lett.* **2001**, *348* (3−4), 161–167.
(37) Vallee, R. A. L.; Tomczak, N.; Kuipers, L.; Vancso, G. J.; van Hulst, N. F. *Phys. Rev. Lett.* **2003**, *91* (3), 038301.
(38) Ram, R. J.; Babic, D. I.; York, R. A.; Bowers, J. E. *IEEE J. Quantum Electron.* **1995**, *31* (2), 399–410.
(39) Weber, W. H.; Eagen, C. F. *Opt. Lett.* **1979**, *4* (8), 236.
(40) Gould, T. J.; Gunewardene, M. S.; Gudheti, M. V.; Verkhusha, V. V.; Yin, S.-R.; Gosse, J. A.; Hess, S. T. *Nat. Methods* **2008**, *5* (12), 1027–1030.
(41) Clayton, A. H. A.; Hanley, Q. S.; Arndt-Jovin, D. J.; Subramaniam, V.; Jovin, T. M. *Biophys. J.* **2002**, *83*, 1631–1649.
(42) Stefani, F. D.; Hoogenboom, J. P.; Barkai, E. *Phys. Today* **2009**, *2*, 34–39.
(43) Fisher, B. R.; Eisler, H. J.; Stott, N. E.; Bawendi, M. G. *J. Phys. Chem. B* **2004**, *108* (1), 143–148.
(44) van Driel, A. F.; Nikolaev, I. S.; Vergeer, P.; Lodahl, P.; Vanmaekelbergh, D.; Vos, W. L. *Phys. Rev. B* **2007**, *75*, 035329.

NL803865A